

Giant magneto-optical Kerr rotation observed in CeS single crystals

R. Pittini*

Laboratorium für Festkörperphysik, Eidgenössische Technische Hochschule, Hönggerberg, 8093 Zürich, Switzerland

J. Schoenes

Institut für Halbleiterphysik und Optik, Technische Universität Braunschweig, Mendelssohnstr. 3, 38106 Braunschweig, Germany

P. Wachter

Laboratorium für Festkörperphysik, Eidgenössische Technische Hochschule, Hönggerberg, 8093 Zürich, Switzerland

(Received 21 October 1996)

We present the magneto-optical polar Kerr spectra of CeS single crystals, measured at 1.5 K in a field of 10 T. These spectra are dominated by a sharp and giant negative Kerr rotation peak of -22.08° detected at the photon energy of 3.04 eV. This peak is the second largest measured Kerr rotation (after the record of 90° detected recently on CeSb) in spite of the low magnetic moment of $0.31\mu_B/\text{Ce}$ achieved in the CeS crystal under the experimental conditions. From these values, we find that CeS has the largest observed specific Kerr rotation, which is as high as $71.23^\circ/\mu_B$. Similar sharp negative peaks were observed in the magneto-optical Kerr rotation spectra of CeSe and CeTe at 2.60 and 1.99 eV, respectively. All these Kerr rotation peaks arise from $4f \rightarrow 5d$ transitions from the $4f$ component of a p - f mixed state, as understood from the transition energies and comparing the total weight of the off-diagonal conductivity with the sample magnetization. [S0163-1829(97)05912-2]

INTRODUCTION

Cerium carries a single $4f$ electron. But, though apparently simple, the $4f^1$ state in cerium compounds presents many anomalous and fascinating properties due to f -band interactions. Among the cerium-based materials one finds heavy-fermion systems, intermediate valent compounds, Kondo metals, and Kondo insulators. To correctly understand the electronic structure and the magnetic properties of these materials, it is necessary to know the exact energy position of the $4f^1$ state and the relevance of the f -band mixing effects. In this light, magneto-optics is an important spectroscopic tool for the study of the f state in rare-earth and actinide compounds.¹ The magneto-optical signal is proportional to the joint density of states and the coupled spin polarization of the electronic states involved in the optical transition.² For this reason, the largest observed magneto-optical Kerr angles arise from $f \rightarrow d$ transitions.³ But while the transitions between f and d states have a strong magneto-optical signal, in optical spectroscopy the signal of the f states nearly vanishes in the background of the strong band-to-band transitions. In fact, in the diagonal conductivity, the oscillator strengths of the transitions that involve quasilocalized f states are very small.⁴

Among the cerium compounds, the cerium monochalcogenides are distinguished for their simplicity. They crystallize in the cubic rock-salt structure and their electronic configuration is characterized by a full valence p band, formed from anionic orbitals, a conduction $5d$ band filled with one electron per formula unit⁵ and one localized $4f$ electron per formula unit. The temperature dependence of the electrical resistivity of the cerium monochalcogenides exhibits Kondo behavior,⁶ indicating nonnegligible d - f mixing. Furthermore, the cerium monochalcogenides order antiferromag-

netically below 8.3, 5.4, and 2.2 K for CeS, CeSe, and CeTe, respectively.⁷ The saturation sublattice moments are reduced from the value of $0.71\mu_B/\text{Ce}$, expected for the doublet Γ_7 ($j_z=5/6$), found to be the $4f^1$ crystal-field ground state in the cerium monochalcogenides from magnetic susceptibility and specific-heat measurements.⁸ The saturation sublattice moments are $0.57\mu_B/\text{Ce}$ for CeS,⁹ $0.56\mu_B/\text{Ce}$ for CeSe, and $0.35\mu_B/\text{Ce}$ for CeTe.¹⁰ To investigate the nature of the $4f^1$ state and the above listed anomalies connected with it in the cerium monochalcogenides, we have measured the magneto-optical polar Kerr effect of CeSe,¹¹ CeTe, and CeS (this work).

EXPERIMENTAL METHODS

Single crystals of CeS were grown by mineralization at a temperature just below the melting point. This method presents the advantage of a minor occurrence of defects in the crystal as compared with the sample growth from the gas phase. The structure and the lattice constant of the single crystals were checked by an x-ray analysis. In addition, measurements of the magnetic susceptibility, the electrical resistivity,⁶ and the Hall effect⁵ confirmed that the single crystals were of the desired quality. Yet, metallic cerium compounds are strongly subjected to oxidization on the surface. Therefore, the single crystals used in the measurements presented here were cleaved, transferred into the cryostat, and measured in an inert atmosphere. The samples were parallelepipeds of typically $2 \times 3 \times 3 \text{ mm}^3$.

The setup of the magneto-optical spectrometer used in this study is shown in Fig. 1. The light emitted from the source becomes monochromatic after passing through a dispersive Zeiss monochromator and is imaged on the polarizer P by a spherical mirror. The monochromatic linearly polar-

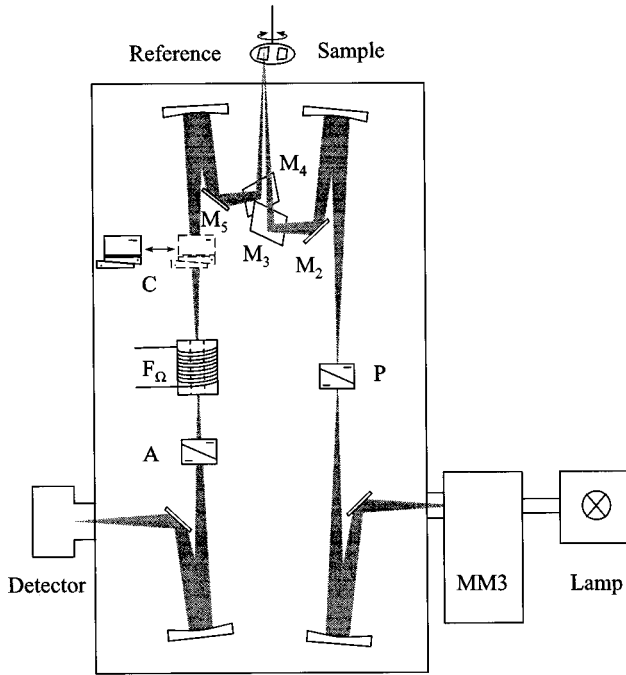


FIG. 1. The setup used for the measurements of the magneto-optical polar Kerr effect.

ized light is then deflected into the cryostat and imaged onto the sample. The light beam is then reflected under an angle of incidence of 2° by the sample or the reference, both mounted on a dish on the sample holder. Half-turn rotations of the dish allow one to switch between sample and reference without changing the optical adjustment of the measurement. Finally, the polarization of the reflected light is analyzed for every wavelength using a phase shifter C and an analyzer A . The use of a Faraday modulator F_Ω allows for noise suppression through a lock-in technique. Three different light sources were used to cover the spectral range from 0.23 to 5.8 eV, i.e., a Global glower (0.23–0.3 eV), a halogen filament in quartz bulb (0.3–2.5 eV), and a xenon high-pressure lamp (2.5–5.8 eV). The dispersive Zeiss monochromator $MM3$ has an optical aperture ratio 1/10. Comparing $MM3$ to grating monochromators with equivalent aperture, the dispersive monochromator has the advantages of considerably smaller dimensions and no higher-order terms that arise from the reflection of light onto a grating. However, the energy resolution of a dispersive monochromator is lower than that of a grating monochromator. For the magneto-optical experiments presented here, a typical energy resolution of 0.01 eV has been estimated for the dispersive monochromator $MM3$. Spherical MgF_2 -coated Al mirrors are used to achieve a 1-to-1 image of the monochromator slit onto the sample and of the sample onto the detector. In contrast to optical lenses, the mirrors do not cause any chromatic aberration of the light spot in the focus and their use can easily be extended into the IR. Plane Al mirrors (M_2 to M_5) turn the light beam from horizontal on the optical table to vertical in the cryostat and again horizontal on the optical table. Mirrors are optically isotropic, but the difference in the reflection coefficients for polarizations in the plane of incidence (ρ_p) or perpendicular to it (ρ_s) may influence the light polarization. The optical setup (Fig. 1) has been designed in a way that the mirrors

placed after the reflection onto the sample mainly compensate the polarization effects of the mirrors placed before the reflection onto the sample. In addition, the axial symmetry of the polar magneto-optical configuration allows the cancellation of all the effects of the mirrors by subtracting the polarization measurements performed in both field directions. As detector, photovoltaic InSb and Si were used between 0.23 and 1.2 eV and 1.2 and 1.6 eV, respectively. A photomultiplier was used for photon energies between 1.6 and 5.3 eV. Photoconductive detectors need a ground line with the inconvenience that a noise signal is induced in it from the oscillating magnetic field of the Faraday cell.

To cool the sample, an optical ^3He cryostat was used. It enables temperatures down to 0.3 K, but below about 3.5 K, a strong ^3He boiloff is regularly observed down to 1 K. For optical measurements, this represents a serious disadvantage, since the noise of the optical measurement is enhanced when the index of refraction of the exchange gas in the sample space fluctuates around its mean value. Therefore, for the measurements between 1.5 and 2.14 K, we preferred to use ^4He as exchange gas instead of ^3He . ^4He is very stable in the superfluid phase below the λ point at 2.14 K.

The sample is positioned in the center of the superconducting magnet that consists of several concentric NbTi and Nb_3Sn solenoids. The magnet allows for fields up to 13.2 T and can be decoupled from the power supply. The optical access is situated at the bottom of the cryostat through strain-free mounted optical windows.

THEORY

The magneto-optical effect consists in an axial anisotropy, which is connected with the magnetization of the sample. The application of an external field magnetizes the sample along the field direction and thus establishes the direction of the axial anisotropy. As any kind of anisotropy, also the magneto-optical anisotropy can be measured with polarized light. Finally, the experimental results are interpreted in terms of the optical conductivity tensor. The very large magneto-optical signals observed recently in CeSb ,³ as well as in CeS , do not allow one to use the usual approximative expressions, which relate the optical and magneto-optical spectra to the off-diagonal conductivity $\tilde{\sigma}_{xy}$.

The exact expression for the off-diagonal conductivity follows from the complex circular optical conductivities

$$\tilde{\sigma}_\pm = i \frac{\omega}{\pi} \frac{\tilde{\rho}_\pm}{(1 - \tilde{\rho}_\pm)^2} = \tilde{\sigma}_{xx} \pm i \tilde{\sigma}_{xy}, \quad (1)$$

where the reflection coefficients $\tilde{\rho}_\pm$ for the right (+, rcp) and left (−, lcp) circular light polarizations carry the information on the magneto-optical effects under the form of a complex phase, which vanishes in the absence of a sample magnetization and changes the sign when the field direction is reversed. Therefore, the reflection coefficients can be written as

$$\tilde{\rho}_\pm = \tilde{\rho} e^{\mp i(\theta_K - iD_K)} \quad (2)$$

with

$$\tan \varepsilon_K = \text{Tanh } D_K, \quad (3)$$

as follows by comparing the polarizations of the light beam before and after the reflection onto the magnetized sample. The formulation (2) for the circular reflection coefficients is, in its simplicity, the key for the derivation of an exact relation between the off-diagonal conductivity and the magneto-optical Kerr signal.

It is convenient to separate the optical from the magneto-optical effects by using two different complex phases $\tilde{\gamma}$ and $\tilde{\delta}_K$, defined as $\tilde{\rho} = e^{i\tilde{\gamma}}$ and $\tilde{\delta}_K = \theta_K - iD_K$. Then, the circular optical conductivities take the form

$$\tilde{\sigma}_{\pm} = i \frac{\omega}{2\pi} \frac{1}{\cos(\tilde{\gamma} \mp \tilde{\delta}_K) - 1}. \quad (4)$$

Using Eq. (1), the diagonal and off-diagonal conductivities are found to be given by

$$\begin{aligned} \tilde{\sigma}_{xx} &= \frac{i\omega}{2\pi} \frac{\cos\tilde{\gamma} \cos\tilde{\delta} - 1}{(\cos\tilde{\gamma} - \cos\tilde{\delta})^2}, \\ \tilde{\sigma}_{xy} &= -\frac{\omega}{2\pi} \frac{\sin\tilde{\gamma} \sin\tilde{\delta}}{(\cos\tilde{\gamma} - \cos\tilde{\delta})^2}. \end{aligned} \quad (5)$$

The optical constants can now be introduced into the diagonal and off-diagonal optical conductivities through

$$\begin{aligned} \cos\tilde{\gamma} &= \frac{1}{2} \left(\tilde{\rho} + \frac{1}{\tilde{\rho}} \right) = \frac{\tilde{n}^2 + 1}{\tilde{n}^2 - 1}, \\ \sin\tilde{\gamma} &= \frac{1}{2i} \left(\tilde{\rho} - \frac{1}{\tilde{\rho}} \right) = \frac{2i\tilde{n}}{\tilde{n}^2 - 1}. \end{aligned} \quad (6)$$

The optical conductivities become

$$\begin{aligned} \tilde{\sigma}_{xx} &= \frac{i\omega}{2\pi} (\tilde{n}^2 - 1) \frac{(\tilde{n}^2 + 1)\cos\tilde{\delta}_K - (\tilde{n}^2 - 1)}{[(\tilde{n}^2 - 1)\cos\tilde{\delta}_K - (\tilde{n}^2 + 1)]^2}, \\ \tilde{\sigma}_{xy} &= -\frac{i\omega}{\pi} \tilde{n}(\tilde{n}^2 - 1) \frac{\sin\tilde{\delta}_K}{[(\tilde{n}^2 - 1)\cos\tilde{\delta}_K - (\tilde{n}^2 + 1)]^2}. \end{aligned} \quad (7)$$

For *small Kerr rotations and ellipticities*, one sets $\cos\tilde{\delta}_K = 1$ and $\sin\tilde{\delta}_K = \theta_K - i\varepsilon_K$ and the traditional formulations¹

$$\begin{aligned} \tilde{\sigma}_{xx} &\approx \frac{i\omega}{4\pi} (\tilde{n}^2 - 1), \\ \tilde{\sigma}_{xy} &\approx -\frac{i\omega}{4\pi} \tilde{n}(\tilde{n}^2 - 1)(\theta_K - i\varepsilon_K) \end{aligned} \quad (8)$$

are recovered. The diagonal optical conductivity in Eq. (8) is unaffected by the sample magnetization and the off-diagonal conductivity takes the usual form¹

$$\begin{aligned} \sigma_{1xy} &\approx -\frac{\omega}{4\pi} (B\theta_K + A\varepsilon_K), \\ \sigma_{2xy} &\approx -\frac{\omega}{4\pi} (A\theta_K - B\varepsilon_K), \end{aligned} \quad (9)$$

with

$$\begin{aligned} A &= n^3 - 3nk^2 - n, \\ B &= -k^3 + 3n^2k - k. \end{aligned} \quad (10)$$

For *large Kerr rotations and ellipticities* (above 10°), no approximative expressions can be used. One has to use *exact* formulas that, to our knowledge, have not been derived yet. The exact formulas for the real and imaginary parts of the off-diagonal conductivity are [as follows directly from Eq. (7)]

$$\sigma_{1xy} = -\frac{\omega}{\pi} [(Bc + Ad)s_1 + (Ac - Bd)s_2], \quad (11)$$

$$\sigma_{2xy} = -\frac{\omega}{\pi} [(Ac - Bd)s_1 - (Bc + Ad)s_2],$$

where A and B are defined in Eq. (10) and c and d follow from

$$c - id = \frac{1}{(a + ib)^2} = \frac{a^2 - b^2}{(a^2 + b^2)^2} - i \frac{2ab}{(a^2 + b^2)^2}, \quad (12)$$

where

$$\begin{aligned} a + ib &= (n^2 - k^2 - 1)c_1 + 2nkc_2 - n^2 + k^2 - 1 \\ &\quad + i[(n^2 - k^2 - 1)c_2 - 2nkc_1 + 2nk] \end{aligned} \quad (13)$$

is the denominator of Eq. (7) and

$$\begin{aligned} c_1 + ic_2 &= \cos\tilde{\delta}_K = \frac{\cos\theta_K \cos\varepsilon_K}{\sqrt{\cos 2\varepsilon_K}} + i \frac{\sin\theta_K \sin\varepsilon_K}{\sqrt{\cos 2\varepsilon_K}}, \\ s_1 - is_2 &= \sin\tilde{\delta}_K = \frac{\sin\theta_K \cos\varepsilon_K}{\sqrt{\cos 2\varepsilon_K}} - i \frac{\cos\theta_K \sin\varepsilon_K}{\sqrt{\cos 2\varepsilon_K}}. \end{aligned} \quad (14)$$

The result (11)–(14) is valid for any magnitude of the measured Kerr effect.

From Eqs. (1)–(3) it follows that, at optical frequencies, the Kerr ellipticity *never* reaches the value of $\pm 45^\circ$. Indeed, a Kerr ellipticity $\varepsilon_K = \pm 45^\circ$ is equivalent to a Kerr dichroism $D_K = \infty$. An infinite Kerr dichroism requires from the circular reflection coefficients $\tilde{\rho}_+ = 0$ and $\tilde{\rho}_- = \infty$ (or inversely), except when the field-free reflection coefficient $\tilde{\rho}$ itself vanishes.

RESULTS AND DISCUSSION

Optics

In Fig. 2, we show the optical reflectivity measured under near-normal incidence on cleaved single crystals of CeS,¹² CeSe,¹¹ and CeTe (Ref. 13) in the energy range between 0.03 and 12.4 eV. Below 3 eV, the optical reflectivity of the cerium monochalcogenides is dominated by the signal of the conduction electrons. Going from CeTe to CeS, the energies of the screened plasma edge increase and the plasma minimum of the reflectivity becomes deeper. The structures observed in the reflectivity above 3 eV mainly arise from p (chalcogen) $\rightarrow 5d$ (cerium) transitions.

The optical constants of CeS, CeSe, and CeTe were obtained through a Kramers-Kronig transformation of the measured reflectivity curves. For this purpose, the reflectivity has

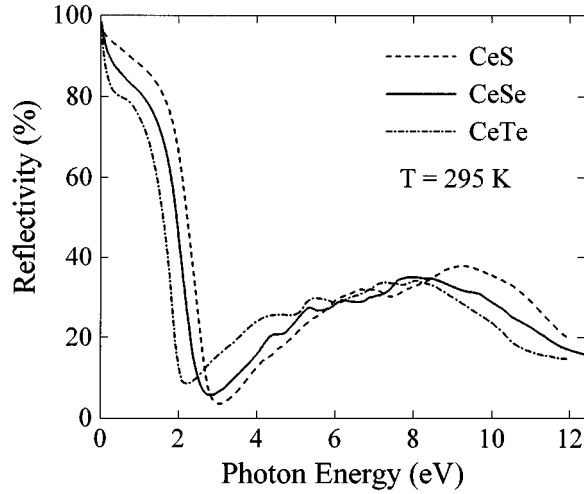


FIG. 2. Near normal incidence reflectivity of the cerium monochalcogenides in the energy range up to 12.4 eV.

been extrapolated into the infrared to $\hbar\omega=0$ with a Hagen-Rubens fit, taking into account the dc conductivity. The UV part has been extrapolated using a ω^{-2} law above 12 eV and a ω^{-4} law above 20 eV. In Fig. 3 we show the absorptive part $\sigma_{1,xx}(\omega)$ of the optical conductivity, separated into intraband and interband contributions in order to better recognize the structures from weak interband transitions.

The parameters that describe the optical properties of the conduction electrons were determined from a combined Drude fit of the dispersive and the absorptive dielectric functions ε_1 and ε_2 . The fit of ε_1 or ε_2 alone is misleading, because the signal of an interband transition near the coupled plasma energy mixes with the Drude-like contribution of the dielectric functions. The results of the simultaneous Drude fit of ε_1 and ε_2 are summarized in Table I. From the unscreened plasma energy, the value of N/m^* for the conduction electrons can be obtained. The normal part of the Hall effect⁵ corresponds to the contribution of one conduction electron per formula unit within a one-band model. From this value, we find that the effective mass determined from the un-

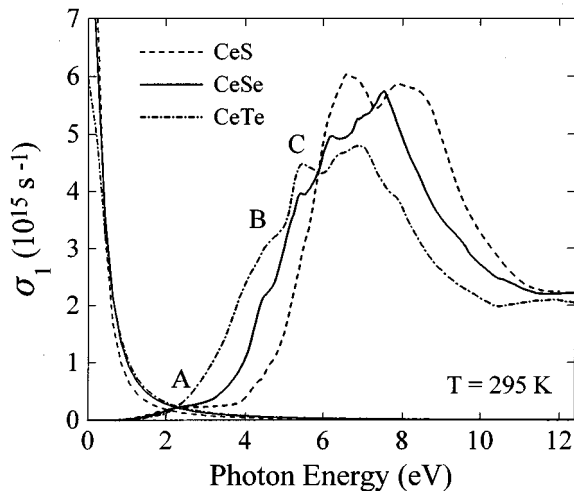


FIG. 3. Absorptive part $\sigma_{1,xx}$ of the diagonal optical conductivity separated in intraband and interband contributions.

TABLE I. Density $N_0=4/a^3$ of the formula units, results of the Drude fit and Fermi energies of the cerium monochalcogenides.

	N_0 (10^{22} cm $^{-3}$)	$\hbar\omega_p$ (eV)	$\hbar\gamma$ (eV)	E_F (eV)
CeS	2.073	5.04	0.23	2.45
CeSe	1.859	4.86	0.38	2.36
CeTe	1.554	4.66	0.47	2.30

screened plasma energy $\hbar\omega_p=(4\pi Ne^2/m^*)^{1/2}$ is equal to nearly one free electron mass for all three materials. This must be understood as the mean effective mass of the occupied $5d$ states and it is not necessarily equal to the effective mass of the conduction carriers at the Fermi level. The Fermi energy (Table I), as measured from the bottom of the $5d$ conduction band, follows from

$$E_F = \frac{\hbar^2 k_F^2}{2m^*} = \frac{1}{8e^2} \left(\frac{9\pi}{4} \right)^{1/3} a (\hbar\omega_p)^2, \quad (15)$$

where a is the lattice constant. Going from CeTe to CeS, the scattering rate decreases and the Fermi energy increases, reflecting the broadening of the conduction band with increasing radial d - d overlap.

In the interband contributions to the optical conductivity, the most prominent feature is a broad and structured peak observed between 4 and 10 eV. This is mainly the signal of the p (chalcogen) $\rightarrow 5d$ (cerium) transitions. From CeTe to CeS, the binding energy of the valence p band increases. As a consequence, the absorption energies of the $p \rightarrow d$ transitions increase, going from CeTe to CeS, as is observed in the reflectivity and conductivity spectra. For CeS, the two main peaks observed in the optical conductivity were assigned¹² to the two transitions $3p \rightarrow 5d(t_{2g})$ and $3p \rightarrow 5d(e_g)$. From them, the value of 1.6 eV was derived for the crystal-field splitting of the conduction band.¹² Similarly, the values of 1.5 and 1.4 eV can be determined for the crystal-field splitting of the conduction band in CeSe and CeTe, respectively, from the broad $p \rightarrow d$ transitions (Fig. 3). We find that the magnitude of the crystal-field splitting of the $5d$ band in the cerium monochalcogenides is comparable to that in the europium monochalcogenides.

It should be noticed that the interband part of the optical conductivity of the cerium monochalcogenides above 4 eV is different from the curves published previously in Ref. 11. In those previous data, the UV extrapolation of the reflectivity used for the computation of the Kramers-Kronig transformation of the reflectivity was interrupted at 18 eV already. As a consequence, the effective number N_{eff} of optically excited charge carriers was found to be about 30% lower than expected for the $p \rightarrow d$ transitions. The effective number N_{eff} of excited carriers,

$$N_{\text{eff}}(E) = \frac{2m_e}{\hbar\pi e^2} \int_0^E \sigma_{1,xx}(E') dE', \quad (16)$$

obtained from the new Kramers-Kronig calculation is shown in Fig. 4. The signal of the one conduction electron per formula unit can be distinguished below 4 eV. Between 4 and 12 eV, the contribution of $6p$ electrons is recognized and N_{eff} tends to increase further above 12 eV. The weak shoul-

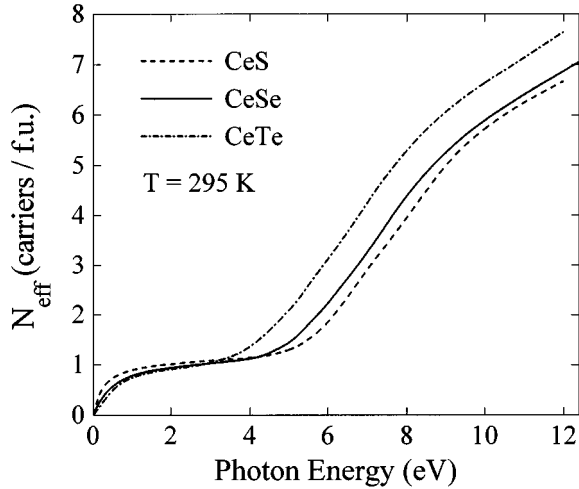


FIG. 4. Effective number of the optically excited electrons as a function of the energy of the incident photons.

der A (Fig. 3) observed in the interband part of the optical conductivity around 2.5 eV as the first absorption sits at about 1 eV higher energy than the onset of electronic interband transitions. The plasmon is screened just below the energy of this absorption A and the plasma minimum of the reflectivity is concomitant with the absorption A. The oscillator strength of the transition A is small and increases from CeTe to CeS. No contribution of the peak A of the optical conductivity can be recognized in N_{eff} . The small oscillator strength of the feature A is indicative of a $4f \rightarrow 5d$ transition.^{4,12} But a definitive assignment shall be made on the basis of the magneto-optical spectra and the off-diagonal

TABLE II. Sample properties related to the Kerr rotation peak.

	$\hbar\omega_{\text{max}}$ (eV)	$-\theta_{K\text{max}}$ (deg)	$R(\omega_{\text{max}})$ (%)	M (μ_B/Ce)	$-\theta_{K\text{max}}/M$ [deg/ (μ_B/Ce)]
CeS	3.04	22.08	3.5	0.31	71.23
CeSe	2.60	5.51	7.4	0.45	12.24
CeTe	1.99	3.32	12.8	0.66	5.03

conductivity, since magneto-optics is selectively sensitive to spin-polarized and spin-orbit split states, while all electrical dipole transitions contribute to the optical signal.

Magneto-optics

The polar magneto-optical Kerr effect measured on CeS, CeSe,¹¹ and CeTe (Ref. 13) is illustrated in Fig. 5. All three spectra are qualitatively very similar. They are dominated by a sharp and large negative Kerr rotation peak of -22.08° , -5.51° , and -3.32° detected at photon energies of 3.04, 2.60, and 1.99 eV for CeS, CeSe, and CeTe, respectively (Table II) with a remarkably small width of 0.1 eV. These Kerr rotation peaks are significant, in particular if one considers the small magnetic moment achieved in the sample at the conditions of the experiment (Table II). Particularly meaningful is the Kerr rotation peak of -22.08° observed in CeS with a magnetic moment of only $0.31\mu_B/\text{Ce}$. This extraordinary peak corresponds to the highest ever observed specific Kerr rotation of $71.23^\circ/\mu_B$ and to the second largest ever measured Kerr rotation after the record of 90° recently detected on CeSb.³ Also, the figure of merit $R \sin^2 2\theta_K$ of the peak in CeS at 3.04 eV is higher than the corresponding

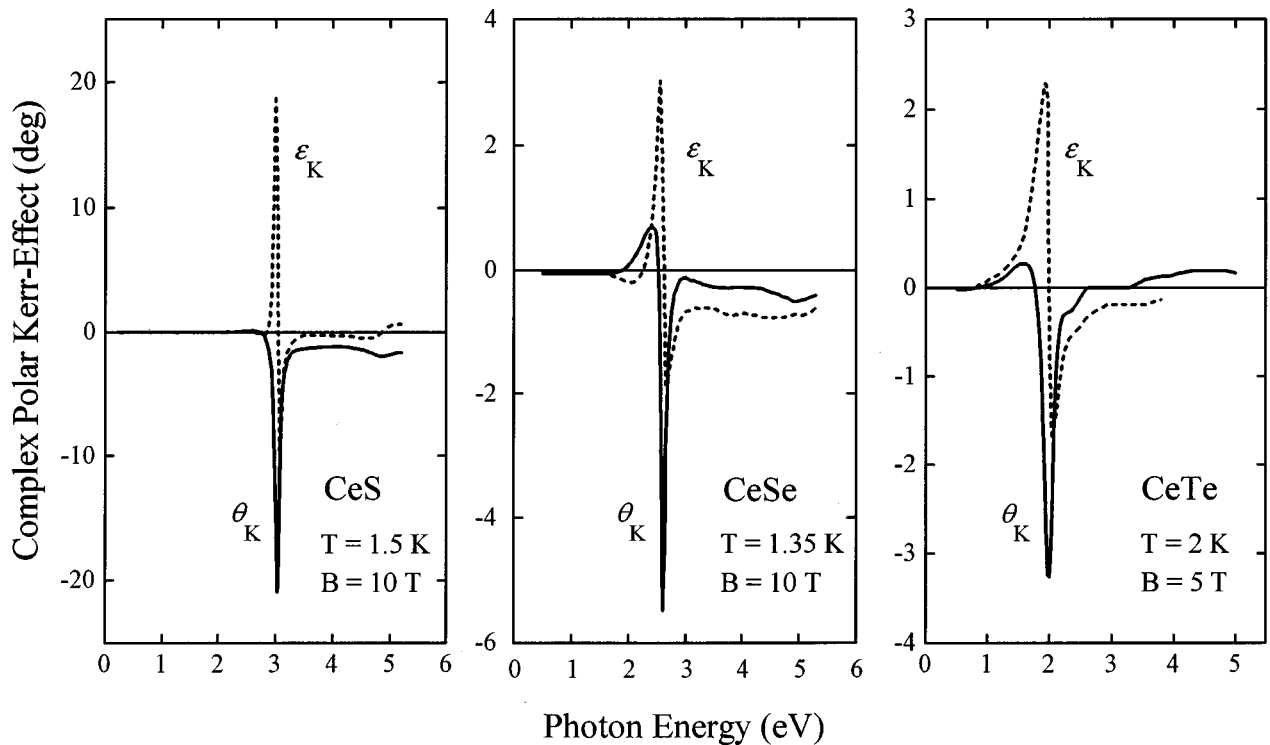


FIG. 5. Energy spectra of the polar magneto-optical Kerr rotation and ellipticity of the cerium monochalcogenides measured at 1.5 K and 10 T, 1.35 K and 10 T, 2 K and 5 T for CeS, CeSe, and CeTe, respectively.

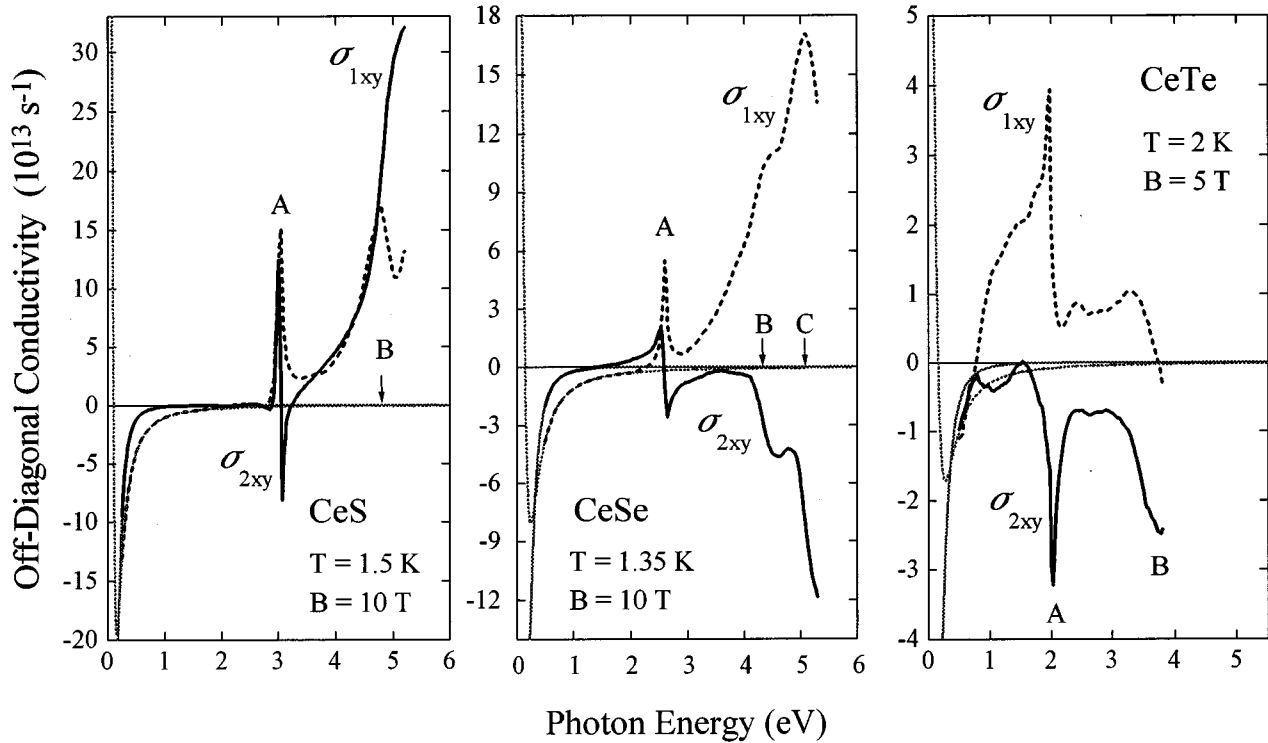


FIG. 6. Real and imaginary parts of the off-diagonal conductivities of CeS, CeSe, and CeTe. Also shown is the fit of the intraband contributions.

figure of merit of the uranium chalcogenides¹⁴ despite the very low reflectivity of CeS at 3.04 eV (Table II). Even more surprising is the observation that the maximum Kerr angle, as compared among the cerium monochalcogenides, is not proportional to the magnetic moment achieved in the sample at the experimental conditions of the magneto-optical measurement, but it is rather complementary to it. In fact, the huge maximum Kerr rotation of -22.08° observed in CeS is 6.65 times the maximum observed on CeTe, but at less than half magnetization as CeTe. This trend is not an effect of the optical constants, since it is also observed in the off-diagonal conductivity, as will be discussed later.

We have calculated the off-diagonal conductivity (Fig. 6) from the measured Kerr rotation and ellipticity spectra and the room-temperature optical constants using the exact relation (11)–(14). We notice that, besides the room-temperature reflectivity curves shown in Fig. 3, we have measured the optical reflectivity also at the conditions of the magneto-optical experiment (at low temperature and in the magnetic field, for photon energies between 0.55 and 5.5 eV) for some of the samples. But no temperature or field dependence of the optical reflectivity could be detected. We conclude that it is legitimate to use the room-temperature values of the optical constants for the determination of the off-diagonal conductivity of the cerium monochalcogenides. This statement is no longer valid for other materials. In CeBi (Ref. 15) and CeSb (Ref. 3), for example, the optical conductivity is strongly temperature and field dependent and follows the changes of the magnetic structure.

From the Hall effect and the parameters of the Drude fit (Table I), the spin polarization $\langle \sigma_z \rangle$ of the conduction electrons could be determined through a fit of the intraband contribution,

$$\tilde{\sigma}_{xy} = \frac{\omega_p^2}{4\pi} \langle \sigma_z \rangle \left[\frac{-\Omega}{\Omega^2 + (\gamma + i\omega)^2} + \frac{P_0}{e\nu_F} \left(1 - \frac{i\omega(\gamma + i\omega)}{\Omega^2 + (\gamma + i\omega)^2} \right) \right], \quad (17)$$

to the off-diagonal conductivity.¹ The skew-scattering frequency Ω of the conduction electrons has been set equal to the spin-orbit parameter $\xi_{SO} = 0.0568$ eV of the 5d band.¹⁶ The mean radial extent of the 5d wave function amounts to 1.81 Å in a purely atomic model. The estimated value of 1.99×10^{-17} s for $P_0/e\nu_F$ makes the second term in Eq. (17) negligible compared to the first term for $\omega \rightarrow 0$. The spin polarization of the conduction electrons was found to amount to -0.61% for CeS at 1.5 K with $B = 10$ T, -7.2% for CeSe at 1.35 K with $B = 10$ T. At $T = 2$ K and $B = 5$ T, the spin polarization amounts to -2.1% for CeTe, -3.4% for CeSe, and only -0.25% for CeS.¹¹ It corresponds to an exchange splitting of the conduction band of 0.048 eV for CeTe, 0.080 eV for CeSe, and only 0.006 eV for CeS, assuming a rectangular density of states of width $W = E_F$. In a field of 10 T we find an exchange splitting of 0.17 and only 0.015 eV of the conduction band in CeSe and CeS, respectively. The spin polarization is anomalous and extremely small in CeS. It probably reflects the lower covalency in CeS compared to the heavier cerium monochalcogenides. The sign of the spin polarization is intended with respect to the external magnetic field. The negative sign found for the spin polarization of the conduction electrons in the cerium monochalcogenides indicates that the exchange energy J_{fd} between the spins of the 4f electrons and the conduction electrons at the Fermi level is negative. In other words, the spins of the conduction electrons are aligned antiparallel to the 4f spins, as would be

expected for the occurrence of the Kondo effect, i.e., antiparallel spin coupling.

In correspondence with the peak Kerr rotation and the weak feature *A* in the optical conductivity, we found a strong and sharp contribution to the off-diagonal conductivity at 3.05, 2.60, and 2.01 eV in CeS, CeSe, and CeTe, respectively. Apart from it, other two magneto-optically active structures are found at 4.78 eV for CeS, 4.32 and 5.08 eV for CeSe, and 3.73 eV for CeTe in the off-diagonal conductivity (Fig. 6). All the observed transitions *A*, *B*, and *C* have a diamagnetic line shape,¹⁷ except in CeTe (Fig. 6). The narrowness and magnitude of the feature *A* indicate that a well localized and highly spin-polarized *f* state is involved in this transition. We therefore assign this structure to a $4f \rightarrow 5d$ transition. Accordingly, the rcp absorption occurs at a higher energy than the lcp absorption (Fig. 6), as expected for a $4f \rightarrow 5d$ transition. The fact that in CeTe the line shape of *A* is different from the other cerium monochalcogenides is astonishing, because at the experimental conditions of $B=5$ T and $T=2$ K the free-ion moment is not saturated in CeTe. Therefore, one cannot assume in CeTe a ground state $|j=\frac{5}{2}, j_z=-\frac{5}{2}\rangle$, which would show a paramagnetic line shape, because in an optical spin-conserving transition into the conduction $5d$ band only the selection rule $\Delta j_z=+1$ can be realized. But we notice that the crystal-field ground state Γ_7 is saturated in CeTe under experimental circumstances. The Γ_7 wave function with the expectation value $-\frac{5}{6}$ for the magnetic quantum number j_z is $|j, j_z\rangle = \sqrt{\frac{1}{6}}|\frac{5}{2}, \frac{5}{2}\rangle + \sqrt{\frac{5}{6}}|\frac{5}{2}, -\frac{3}{2}\rangle$.¹⁹ The possible transitions into the conduction $5d$ band are, for the first component of Γ_7 , the spin-conserving transition $|\frac{5}{2}, \frac{5}{2}\rangle \rightarrow |\frac{3}{2}, \frac{3}{2}\rangle$ with paramagnetic line shape and a weak spin-flip transition to $|\frac{5}{2}, \frac{3}{2}\rangle$, also with paramagnetic line shape. For the second component of Γ_7 , the spin-conserving transition $|\frac{5}{2}, -\frac{3}{2}\rangle \rightarrow |\frac{3}{2}, -\frac{1}{2}\rangle$ with paramagnetic line shape and two weak spin-flip transitions to $|\frac{5}{2}, -\frac{5}{2}\rangle$ and $|\frac{5}{2}, -\frac{1}{2}\rangle$ (yielding a diamagnetic line shape) are possible. Summarizing, the dominant transition is $|\frac{5}{2}, -\frac{3}{2}\rangle \rightarrow |\frac{3}{2}, -\frac{1}{2}\rangle$, yielding a paramagnetic line shape. This transition corresponds to an absorption of right circular polarized light ($\Delta j_z=+1$) and yields a negative contribution to σ_{2xy} , as is indeed observed (Fig. 6). The other important transition contributing to peak *A* in CeTe is $|\frac{5}{2}, \frac{5}{2}\rangle \rightarrow |\frac{3}{2}, \frac{3}{2}\rangle$, which is an absorption of left circular polarized light yielding a positive σ_{2xy} signal with paramagnetic line shape at the same energy as the dominant transition. Essentially, these two contributions mutually cancel in part in peak *A*, so that the magneto-optical weight of *A* is reduced from the optical weight of *A* in CeTe, despite the paramagnetic line shape of the magneto-optical absorption. In the optical experiment performed in the absence of any external magnetic field, all the j_z states $\pm\frac{3}{2}$ and $\pm\frac{5}{2}$ of Γ_7 contribute to the absorption *A*. In CeS and CeSe, the magnetic moment of the Γ_7 crystal field ground state is not saturated yet. All the j_z states of Γ_7 contribute to the magneto-optical absorption yielding a diamagnetic line shape with the dominant transitions $|\frac{5}{2}, -\frac{3}{2}\rangle \rightarrow |\frac{3}{2}, -\frac{1}{2}\rangle$ and $|\frac{5}{2}, \frac{3}{2}\rangle \rightarrow |\frac{3}{2}, \frac{1}{2}\rangle$ for the two states in the Γ_7 doublet with $j_z=-\frac{5}{6}$ (as in CeTe) and $j_z=\frac{5}{6}$, respectively. The lcp absorption occurs at a lower energy, since the state with $j_z=-\frac{5}{6}$ is the ground state of Γ_7 . The saturation of Γ_7 in CeTe also means that CeTe is, under the experimental conditions of $B=5$ T and $T=2$ K, more strongly orbitally polarized than CeS and CeSe at $B=10$ T and $T=1.5$ K in spite of

the stronger crystalline field in the more ionic compounds. The saturation of Γ_7 is strongly hindered by *f*-band mixing effects and by the stronger antiferromagnetic coupling of the spins in CeS and CeSe, and is reached at 1.5 K in the fields of 16 T for CeSe and 27 T for CeS.²⁰

The features *B* and *C* in the off-diagonal conductivity have the same line shape as the structure *A*. They are therefore understood to arise from $4f \rightarrow 5d$ transitions to higher energy final $5d$ states. Interband transitions contribute to the off-diagonal optical conductivity if at least one of the involved states is spin polarized and one is spin-orbit split. A peak in the optical conductivity is found for the optical transitions between states with the same energy slope in the reciprocal space. For the $4f \rightarrow 5d$ transitions, van Hove singularities are expected in the optical conductivity for the absorptions $4f \rightarrow 5d(t_{2g})$ and $4f \rightarrow 5d(e_g)$. Therefore, we assign the transition *A* to the $4f \rightarrow 5d(t_{2g})$ transition, in which the final state $5d(t_{2g})$ is found from band-structure calculations¹⁸ to lie near the Fermi level in these materials. In correspondence to the values found for the $5d$ crystal-field splitting, the transition $4f \rightarrow 5d(e_g)$ is expected in the region 4–5 eV, where we find the peak *B*. Therefore, we assign the magneto-optically active feature *B* to the $4f \rightarrow 5d(e_g)$ transition, confirming the assignments that Schoenes¹² proposed on the basis of the weak structures observed in the optical conductivity of CeS at 2.7 and 4.3 eV. The peak *C* detected in CeSe is thought to arise from a $4f \rightarrow 5d(e_g)$ transition as *B*, since it has the same line shape as *B* and the $5d$ density of states obtained from a band structure calculation¹⁸ shows two peaks split by 0.9 eV in the region of $5d(e_g)$. We notice that in the optical conductivity (Fig. 3) the peaks *B* and *C* are stronger in CeTe than in CeS and CeSe, while the peak *A* follows the opposite trend. But in the off-diagonal conductivity (Fig. 6), both peaks *A* and *B* are strongest in CeS. Since the initial state of the two transitions *A* and *B* is the same, we conclude that in the optical conductivity the contribution of the transition $4f \rightarrow 5d(e_g)$ strongly overlaps with the transition $p(\text{anion}) \rightarrow 5d(t_{2g})$, which in CeTe sets in at lower energy than in CeSe and CeS.

In the Kerr spectra (Fig. 5), we observed that the maximum Kerr rotation is not proportional to the magnetization of the sample (Table II). This anomaly is valid also for the off-diagonal conductivity. For both transitions *A* and *B* the initial state is a $4f$ state, which is not the main $4f$ level, responsible for the sample magnetization, but rather a *p-f* mixed state. From the charge distribution of the *p* and *f* orbitals²¹ the *p-f* mixing is found to be very anisotropic. This leads to a splitting of the *f* character rather than to a dispersion of the *f* character over the valence band, as would occur in the case of an isotropic *p-f* mixing. Thus, in the cerium compounds the *p-f* mixing determines the distribution of the *f* character over the valence band and tunes the strength of the magneto-optical effects. In this light, the initial state of the transition *A* is not the full $4f^1$ level but a *p-f* mixed level, called the “effective” $4f$ level in the original model of the *p-f* mixing.²² Therefore, the parameter that governs the size of the maximum Kerr rotation in CeS, CeSe, and CeTe is the amount of *f* character present in the effective $4f$ level. This is determined by the strength of the *p-f* mixing, which in turn depends on the relative energy difference between the “bare” $4f^1$ and *p* states that participate to

the mixing. Instead, the radial p - f overlap along the $\langle 100 \rangle$ directions is nearly equal in CeS, CeSe, and CeTe, as can be judged from the integration of atomic wave functions.¹⁶ The f character present in the “effective” $4f$ level is found to be largest in CeS. This explains the trend of the magnitude of the Kerr rotation peak A in the cerium monochalcogenides.

A further confirmation of the relevance of the p - f mixing in these materials is the different energy position of the $4f \rightarrow 5d$ transitions of the peaks A and B in the off-diagonal conductivity. In fact, the energy difference between the peaks A in CeS and CeSe is 0.55 eV, and between CeSe and CeTe it amounts to 0.59 eV. For the peaks B , we find the same energy difference of 0.55 eV between CeS and CeSe, while between CeSe and CeTe we find an energy difference of 0.69 eV for the peaks B . The latter value is slightly higher than the energy difference of 0.59 eV found for the peaks A , but the peak B in CeTe appears at the UV limit of the spectrum and we could therefore not determine its exact position. The similar energy differences of the peaks A and B in the series of the cerium monochalcogenides confirms that our assignment of A and B to $4f \rightarrow 5d$ transitions from the same initial state to the two final states $5d(t_{2g})$ and $5d(e_g)$ is correct. The energy differences of 0.55 and 0.59 eV, are too large to be explained only by the widening of the conduction band. Instead, they follow the different energy position of the valence band.

The lines of the $4f \rightarrow 5d$ transitions A in CeS, CeSe, and CeTe are very sharp in the σ_{xy} spectra (Fig. 6), while they are much broader in $\sigma_{1xx}(\omega)$ (Fig. 3). This is not due to a temperature dependence of the relaxation time connected with this absorption [in fact, the feature A in $\sigma_{1xx}(\omega)$ is found to be temperature independent], but it originates from the different signals observed in the diagonal and off-diagonal conductivities. The off-diagonal conductivity σ_{xy} is selectively sensitive only to the optical transitions that involve spin-polarized and spin-orbit split states, while all the electrical dipole transitions contribute to σ_{xx} . In the transition A , the p component of the initial p - f mixed state does not contribute to the magneto-optical signal in CeSe, since the valence band is full and thus cannot be spin polarized. Instead, all the p states contribute to the optical conductivity σ_{1xx} . Therefore, in the magneto-optical spectra, the feature A is sharp, while it is broad in $\sigma_{1xx}(\omega)$.

The large Kerr rotation peaks of CeS, CeSe, and CeTe originate from $4f \rightarrow 5d$ transitions where the initial state is a p - f mixed state, which contains only a small part, only a few percent, of the full $4f^1$ state. A relatively small increase of the f component in the “effective” $4f$ level is sufficient to achieve a giant enhancement of the Kerr rotation in the cerium monochalcogenides. The magneto-optical signal of this transition is strongly enhanced for two reasons. Firstly, the peaks in the off-diagonal conductivity are large because they are very narrow and the oscillator strength is concentrated

within a narrow energy range. Secondly, the transitions A appear at the plasma minimum of the reflectivity, where the particularly low values of the optical constants amplify the signal of the off-diagonal conductivity in the magneto-optical Kerr spectra. The reason for this coincidence of the transitions A with the plasma minimum of the reflectivity is again the anisotropic p - f mixing. In fact, in the cerium monochalcogenides, the anisotropic p - f mixing projects the effective $4f$ level into the gap between the valence p and the conduction $5d$ bands. As a consequence, the optical transition A from this p - f mixed level to $5d(t_{2g})$, which is near the Fermi level, is the lowest-energy interband absorption. The plasma edge is screened by the interband transitions and it is shifted just below the lowest-energy absorption A .

CONCLUSIONS

Very large Kerr rotations were observed in the magneto-optical spectra of the cerium monochalcogenides. In particular, a maximum Kerr rotation of -22.08° , the second largest observed Kerr rotation, was detected on CeS with a magnetic moment of only $0.31\mu_B/\text{Ce}$ achieved in the sample at the experimental conditions. These peaks are assigned to $4f \rightarrow 5d$ transitions, for which the oscillator strength in the off-diagonal conductivity is concentrated in a narrow energy range. Furthermore, this $4f \rightarrow 5d$ transition is observed as the first interband transition and is determinant for the screening of the plasmon. As a consequence, the plasma edge is shifted just below the $4f \rightarrow 5d$ absorption and the corresponding Kerr rotation peaks are strongly enhanced.

The values of the maximum Kerr rotation, as well as the total weight in the off-diagonal conductivity, in CeS, CeSe, and CeTe are not proportional to the sample magnetization. This anomaly is understood within the framework of a strongly anisotropic p - f mixing, in which the effective $4f$ level, the initial state of the interband transition connected with the Kerr rotation peak, contains only a small part of the full $4f^1$ state. We find that the position of the bare $4f^1$ state must be set at much lower energy than in the original p - f mixing model.²² Oppeneer *et al.*²³ came to the same conclusion in the discussion of their LDA+ U calculation, in which the trend of the maximum Kerr rotation of the cerium monochalcogenides is well reproduced. The particularity of the $4f$ state in cerium, among the rare earths, is the large radial extent and the particular energy of the $4f^1$ state. In cerium compounds, the bare $4f^1$ state is immersed in the valence-band states, which makes the f -band hybridization particularly effective.

ACKNOWLEDGMENTS

We thank O. Vogt for fruitful discussions. The technical support of P. Dekumbis, J. Müller, K. Mattenberger, and H. P. Staub is gratefully acknowledged.

*Present address: Research Institute for Scientific Measurements, Tohoku University, Sendai 980, Japan.

¹W. Reim and J. Schoenes, in *Handbook of Ferromagnetic Materials*, Vol. V, edited by E. P. Wohlfahrt and K. H. J. Buschow (North-Holland, Amsterdam, 1988), pp. 133–236.

²J. L. Erskine and E. A. Stern, *Phys. Rev. B* **8**, 1239 (1973).

³R. Pittini, J. Schoenes, O. Vogt, and P. Wachter, *Phys. Rev. Lett.* **77**, 944 (1996); R. Pittini, J. Schoenes, and P. Wachter, *Physica B* (to be published).

⁴J. Schoenes and W. Reim, *J. Less-Common Met.* **112**, 19 (1985).

- ⁵K. Hiraoka, R. Pittini, and P. Wachter, *Physica B* (to be published).
- ⁶J. Schoenes and F. Hulliger, *J. Magn. Magn. Mater.* **63 & 64**, 43 (1987).
- ⁷O. Vogt and K. Mattenberger, in *Handbook on the Physics and Chemistry of Rare Earths*, edited by K. A. Gschneider, Jr., L. Eyring, G. H. Lander, and G. R. Choppin (Elsevier, Amsterdam, 1993), Vol. 17, p. 301.
- ⁸F. Hulliger, B. Natterer, and H. R. Ott, *J. Magn. Magn. Mater.* **8**, 87 (1978).
- ⁹P. Schobinger-Papamantellos, P. Fischer, A. Niggli, E. Kaldis, and V. Hildebrandt, *J. Phys. C* **7**, 2023 (1974).
- ¹⁰H. R. Ott, J. K. Kjems, and F. Hulliger, *Phys. Rev. Lett.* **42**, 1378 (1979).
- ¹¹R. Pittini, J. Schoenes, and P. Wachter, *Physica B* **206 & 207**, 92 (1995).
- ¹²J. Schoenes, in *Moment Formation in Solids*, edited by W. J. L. Buyers (Plenum, New York, 1984), pp. 237–248.
- ¹³W. Reim and J. Schoenes, *J. Magn. Magn. Mater.* **54-57**, 1401 (1986).
- ¹⁴W. Reim, O. E. Hüsser, J. Schoenes, E. Kaldis, and P. Wachter, *J. Appl. Phys.* **55**, 2155 (1984).
- ¹⁵R. Pittini, J. Schoenes, F. Hulliger, and P. Wachter, *Phys. Rev. Lett.* **76**, 3428 (1996).
- ¹⁶F. Herman and S. Skillman, in *Atomic Structure Calculations* (Prentice-Hall, Englewood Cliffs, 1963).
- ¹⁷For the definition of “paramagnetic line shape” and “diamagnetic line shape” cf. Ref. 1.
- ¹⁸N. Kioussis, D. Swearingen, B. R. Cooper, and J. M. Wills, *J. Appl. Phys.* **69**, 5475 (1991); N. Kioussis, B. R. Cooper, and J. M. Wills, *Phys. Rev. B* **44**, 10 003 (1991).
- ¹⁹K. R. Lea, M. J. M. Leask, and W. P. Wolf, *J. Phys. Chem. Solids* **23**, 1381 (1962).
- ²⁰A. Dönni, A. Furrer, P. Fischer, and F. Hulliger, *Physica B* **186-188**, 541 (1993).
- ²¹U. Walter, *Z. Physik B* **62**, 299 (1986).
- ²²H. Takahashi and T. Kasuya, *J. Phys. C* **18**, 2697 (1985).
- ²³P. M. Oppeneer, V. N. Antonov, A. Ya. Perlov, A. N. Yaresko, T. Kraft, and H. Eschring, *Physica B* (to be published).